PAPER • **OPEN ACCESS**

Nano-hillock formation on CaF$_2$ due to individual slow Au-cluster impacts

To cite this article: Gabriel L Szabo *et al* 2021 *Nanotechnology* **32** 355701

View the article online for updates and enhancements.

Nano-hillock formation on CaF$_2$ due to individual slow Au-cluster impacts

Gabriel L Szabo[1] ⓘ**, Markus Lehner**[1]**, Lothar Bischoff**[2] ⓘ**, Wolfgang Pilz**[2]**,
Helmut Muckenhuber**[1]**, Ulrich Kentsch**[2]**, Friedrich Aumayr**[1] ⓘ**,
Nico Klingner**[2] ⓘ **and Richard A Wilhelm**[1,*] ⓘ

[1] TU Wien, Institute of Applied Physics, A-1040 Vienna, Austria
[2] Helmholtz-Zentrum Dresden-Rossendorf, Institute of Ion Beam Physics and Materials Research, D-01328 Dresden, Germany

E-mail: gszabo@iap.tuwien.ac.at and wilhelm@iap.tuwien.ac.at

Abstract

We present a direct way to generate hillock-like nanostructures on CaF$_2$(111) ionic crystals by kinetic energy deposition upon Au-cluster irradiation. In the past, the formation of similar nanostructures has been observed for both slow highly charged ions and swift heavy ions. However, in these cases, potential energy deposition of highly charged ions or the electronic energy loss of fast heavy ions, respectively, first leads to strong electronic excitation of the target material before the excitation energy is transferred to the lattice by efficient electron-phonon coupling. We now show that the kinetic energy deposited by slow single Au-clusters directly in the lattice of CaF$_2$(111) leads to the production of nano-hillocks very similar to those found with slow highly charged and swift heavy ions, with heights between 1 and 2 nm. Our results are in good agreement with previous cluster irradiation studies regarding energy deposition and hence nano-structuring of surfaces, and we present Au-cluster irradiation as novel tool to fine-tune nanostructure formation.

Supplementary material for this article is available online

(Some figures may appear in colour only in the online journal)

1. Introduction

Nanostructuring, a fabrication of surface nano-structures on different materials, is one of the most important applications of ion beam technology and has gained great attention over the last two decades [1–4]. With increasing demand for nanoscale engineering of surfaces, innovative methods such as cluster irradiation, irradiations with slow highly charged ions (HCIs) and swift heavy ions (SHIs) are considered for

material alteration in addition to commonly applied low-energy ion beam techniques.

The processes that induce changes of the surface structure differ and depend on the impinging particle and its properties (like charge-state, kinetic energy, size and species) on the one hand [2, 3] and on the irradiated material/surface on the other hand [1, 4]. While for a low-energy cluster ions, i.e. those were the kinetic energy lies below its binding energy, cluster-solid interaction is confined solely to projectile deposition on the surface [5]. High-energy cluster impact on the contrary can lead to a deformation of the target's atomic lattice and enhanced surface sputtering [6]. For the latter, the energy deposition is primarily dominated by nuclear stopping [7] which corresponds to a direct knock-on impact on target nuclei, leading to a displacement of atoms and lattice vibrations (phonons), respectively. Individual

heavy ions (monomeres) already create collisional cascades in the surface. Atomic clusters made from few atoms, however, may lead to the melting of a larger volume and the damage cannot completely anneal subsequently. The interaction can be seen as an overlap of several energetic cascades at the same time, leading to a high-energy spike on the nanoscale. This results in the formation of nano-structures such as hillock-like protrusions on the surface [8–11] or the formation of craters [12, 13].

Comparable hillock-like structures were also found on various surfaces irradiated with HCIs and SHIs [3]. Unlike the prior mentioned process leading to the formation of nano-structures, the prevailing process here is based on electronic rather than nuclear effects and is called electronic stopping: The energy deposition leads to an excitement of the target's electrons. Subsequently, electron-phonon-coupling leads to nano-melting, rapid thermal expansion and quenching around the impact area and finally to the formation of nano-hillocks. However, metallic surfaces are not susceptible to HCI modification using the potential energy [14, 15], only a modification of metallic surfaces induced by kinetic energy effects was observed by Pomeroy *et al* [16]. Surface modifications were mostly observed on insulating materials (e.g. CaF_2, Al_2O_3, $SrTiO_3$, BaF_2, LaF_3, LiF and others [16–30]) as they are more sensitive to structural modifications induced by electronic excitations due to their large bandgap [31]. While the energy deposition for irradiation with HCIs is surface sensitive and only affects the topmost layers, an irradiation with SHIs, due to the large penetration depth [32], is not desirable for e.g. thin film nanoelectronics.

CaF_2, an earth-alkaline halide, was repeatedly investigated regarding nanostructuring with ion beams. Besides the large set of available data for comparison of nano-hillock creation, CaF_2 is particularly convincing for different applications in microelectronic and optoelectronic devices [33, 34]. Therefore, we selected CaF_2 for our experiments in order to draw a direct comparison with HCIs and with existing data on nano-hillock creation with cluster beams in general.

In this contribution we present experimental results with individual slow ($\sim$15 eV/amu) Au-clusters creating nano-hillocks on a CaF_2(111) surface. Using an atomic force microscopy (AFM) instrument, we are able not only to observe the creation of nano-hillocks, but also to determine a correlation between the cluster size and the height of the hillocks protruding from the surface.

2. Experimental setup

The experiments were performed on CaF_2(111) surfaces (commercially acquired from MaTeck GmbH, Germany), that were freshly cleaved in air. After cleavage of samples with a thickness of roughly 0.5 mm, they were heated up to 400 °C in UHV for at least 3 hours to remove surface contaminants and to improve the already known stability (in air) of the fluorine-terminated surface [24]. The pressure of our UHV system was in the range of 5×10^{-7} mbar during heating.
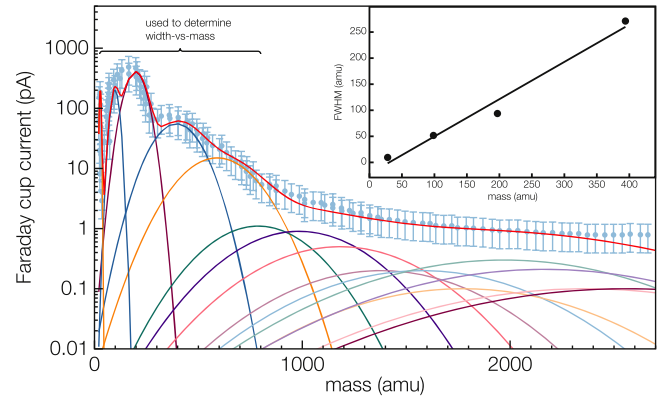

Figure 1. Faraday cup spectrum fit with multiple Gaussian peaks, each representing a different cluster mass. Only the first 5 peaks of the Faraday cup (FC) current were fit to determine the width-versus-mass ratio. The resulting graph is inserted at the top right, where a linear dependence is visible which is used to extrapolate for larger clusters. The fit is applied for the masses up to 2700 amu. As it is shown in figure 4, the full width half maximum (FWHM) broadens with increasing cluster-mass. The error bars represent 10% uncertainty.

Measurements using a tapping-mode AFM (Asylum research cypher scanning probe microscope) were performed under ambient conditions on pristine samples, revealing an atomically flat surface with mono-atomic steps and terrace widths in the order of several hundred nm, that are a result of the cleaving process. Additionally, some areas have shown small clustered islands that appeared to be remaining or re-adhered contaminations of the surface.

The irradiations of the CaF_2 samples were performed at the Ion Beam Center of the Helmholtz-Zentrum Dresden-Rossendorf using a focused ion beam (FIB) equipped with a mass-separated ion column CANION 31M+ (Orsay Physics). Gold clusters Au_a^+ ($a = 1$–10) were extracted from a liquid metal alloy ion source [35] working with $Au_{82}Si_{18}$ as source material. All clusters were accelerated to the same final energy of 30 keV. A Faraday cup (FC) spectrum of the extracted ion-cluster beam recorded using an $E \times B$ filter in the FIB colum is shown in figure 1. The total FC current as a function of the cluster-mass is fit with multiple Gaussian peaks, each representing one specific cluster mass (which is widened in the $E \times B$ filter). To determine the width-to-mass ratio without using it as a free parameter, the first 5 peaks were fit separately. These peaks correspond to Si^+, Au^+, Si^{2+}, Au^{2+}, and Au_2^+. They are well distinguishable (note the log scale) and enable the determination of the individual peak widths. The peak widths are shown in the inset in figure 1 and follow a linear dependence on the cluster-mass. This linear fit is further extrapolated for larger clusters. Using the software *fityk* [36], the total FC current is fit with multiple Gaussians, in a way that only the peak heights are free fit parameters, whereas the mean mass per peak is given by the Au-cluster-size and the width follows from the extrapolation explained above.

For our experiment, CaF_2 was irradiated with different fluences ranging from 1×10^{10} to 1.3×10^{12} ions cm^{-2} of cluster-sizes Au_1^+, Au_2^+, Au_3^+, Au_{5-7}^+ and Au_{9-10}^+. The
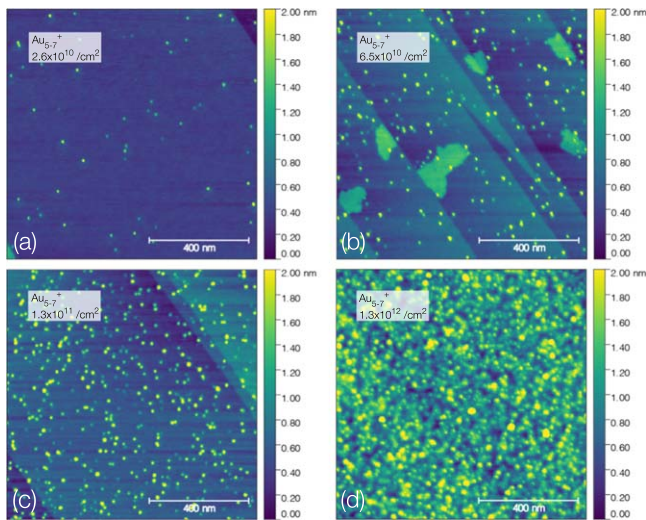
Figure 2. AFM tapping-mode images of a $CaF_2(111)$ surface after irradiation with 30 keV Au_{5-7}^+-clusters. Panel (a)–(d) show the sample irradiated with different fluences: (a) 2.6×10^{10} ions cm^{-2}, (b) 6.5×10^{10} ions cm^{-2}, (c) 1.3×11^{11} ions cm^{-2} and (d) 1.3×12^{12} ions cm^{-2}. It can be seen that the number of hillocks increases with increasing fluence, indicating that they originate from ion cluster irradiation.
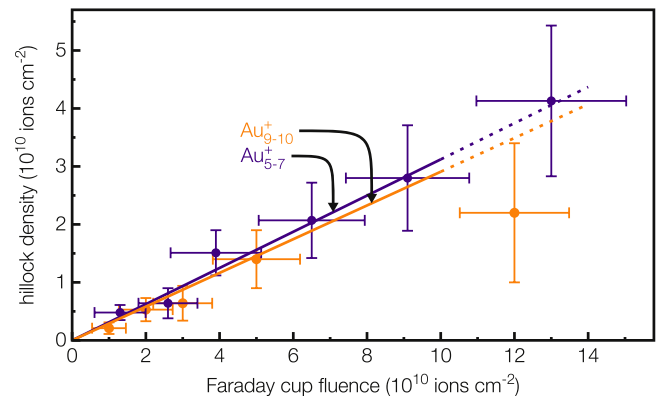

Figure 3. Hillock density compared to the applied cluster fluence, here as an example for Au_{5-7}^+ and Au_{9-10}^+. The incline of the graphs marks the efficiency (hillock/cluster), which was found to be in the range of $20-30\%$, meaning only about every 5th cluster creates a nano-hillock. For the fit, only fluences below 10×10^{10} cm^{-2} were taken into account, to exclude any overlapping double hits. The error bars for the hillock density represent the error of the mean value (in this case $\sqrt{N}$; N: number of hillocks), whereas the error bar for the fluence determined from the ion current in a Faraday cup represents an error of 10%. The error of irradiation area is expected to be negligible in a FIB setup.

irradiations and fluence series were performed on two samples on different areas on the surface. This makes an analysis of the different irradiated areas more reproducable, since the pristine surfaces for each irradiated area are comparable. After irradiation, the samples were inspected with AFM under ambient conditions at TU Wien. For the measurements, the AFM was again operated in tapping mode, using Olympus Micro Cantilever OMCL-AC240TS-R3 tips, with a spring constant of about $2 \, \text{N m}^{-1}$.

3. Results and discussion

As it was already observed in [17, 18], hillock-like nano-structures were found to be protruding from the $CaF_2(111)$ surface. Figure 2 shows topographic AFM images of a $CaF_2(111)$ surface after irradiation with Au_{5-7}^+-cluster, where the creation of mostly round and randomly distributed nano-structures on the surface is observed. To make sure that the nano-hillocks are induced by cluster-irradiation (i.e. they are not contamination residues), the sample was irradiated with different fluences at different positions on the surface. The applied fluences in figure 2 are as follows: (a) 2.6×10^{10} ions cm^{-2}, (b) 6.5×10^{10} ions cm^{-2}, (c) 1.3×11^{11} ions cm^{-2} and (d) 1.3×12^{12} ions cm^{-2}. With increasing fluence, it can be seen that also the number of hillocks increases. This indicates that the nano-hillocks originate from a process induced by the ion cluster irradiation. For the analysis, only the samples irradiated with fluences below $\sim 10^{11}$ ions cm^{-2} were used, where a clear distinction of each individual hillock is possible. For higher fluences the probability for double and multiple hits increases significantly and nano-hillocks start to overlap, which can be seen in figure 2(d). For fluences in the range of 1×10^{12} ions cm^{-2} and above, a quantitative analysis of individual features is not possible, but nevertheless those

measurements are helpful to link the origin of these structures to the cluster-irradiation. The islands connected to step edges seen in figure 2(b) were already observed in measurements on pristine CaF_2 and are hence not ion-induced features. The AFM images were analyzed with respect to the hillock density (see figure 3), hillock height (see figure 4), and volume (see supplementary information figure 1 (available online at stacks.iop.org/NANO/32/355701/mmedia)). For sufficient statistics, about $100-150$ hillocks per measurement were analyzed. A systematical error occurs in the process of measuring the hillock-volume in the order of $100-200$ nm^3, which is caused by the convolution and tip shape, which depends on the type of tip used. Contrary to the volume, the height of the hillocks is less affected by this fact or by the tip geometry. The surface roughness of the pristine surface is well below 0.5 nm. The areal density of the hillocks was found to be only about 20%–30% of the applied cluster fluence, meaning that only about every fifth cluster creates a nano-hillock (see figure 3). Please note, that there exists a large uncertainty of the applied (nominal) fluence in the experiment (not shown in figure 3). Since the irradiation was performed in a FIB and comparatively low fluences were used with respect to typical FIB experiments, the sample may not be homogeneously irradiated as a consequence of beam blanking and sweeping procedures. The FIB irradiation was made in $400 \times 400 \, \mu m^2$ scan fields with only one sweep. The fluence was adjusted varying the pixel dwell time. To define a fluence as low as 10^{10} ions cm^{-2} in a 4096×4096 pixel field, only every fifth pixel was irradiated using an ion current of 300 fA for the Au_{10}^+ cluster beam for instance (further information can be found in the supplementary information figure 2). We therefore assume an unknown offset to the nominal fluence, which makes a definitive evaluation of the hillock production efficiency difficult.
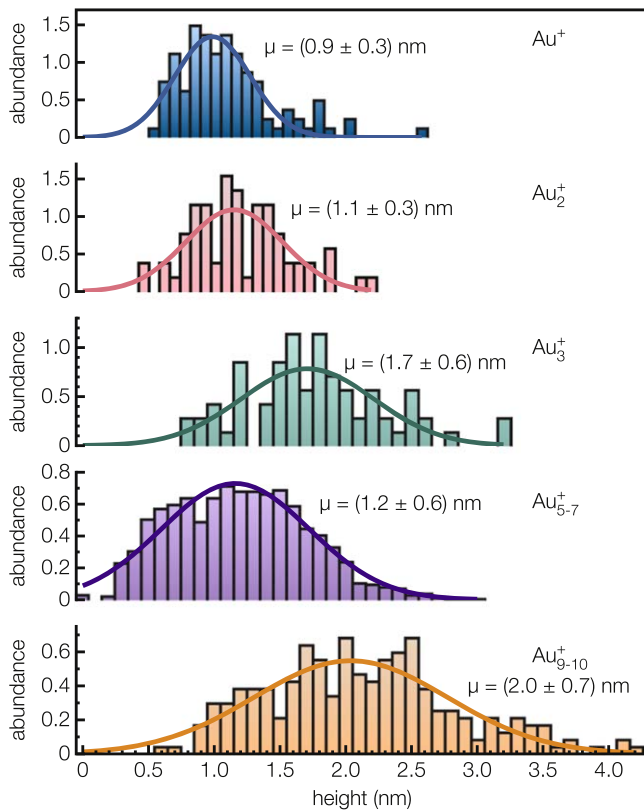
Figure 4. Frequency distributions of hillock heights for different cluster sizes of the CaF$_2$(111) crystal irradiated with 30 keV Au$_1^+$, Au$_2^+$, Au$_3^+$, Au$_{5-7}^+$ and Au$_{9-10}^+$. The mean values μ_{Au_a} (a indicating the cluster size) are obtained by fitting a Gaussian to the data. One can see, that the widths (FWHM) of the distributions broadens with increasing cluster size. This is due to extraction from the LMAIS, where the separation of different cluster sizes gets weaker with increasing cluster mass. For details, please see the text and figures 1 and 6.

The hillock height distribution for the different cluster-sizes is shown in figure 4. The mean hillock height was determined by fitting a Gaussian function to the abundance. Noticeable in this graph is the full width at half maximum of the distributions, which broadens with increasing cluster-sizes. As mentioned before, this broadening is a result of a decreasing mass-resolution in the $E \times B$ filter for increasing mass.

From the data in figure 1 a cluster-size spectrum is extracted and shown in figure 5 for Au$_5^+$ and Au$_{10}^+$. When selecting Au$_5$-clusters, not only Au$_5^+$ (36%) contributes to the FC current, but also Au$_4^+$ (~8%), Au$_6^+$ (~28%) and Au$_7^+$ (~10%). Comparing the Au$_5^+$ with the Au$_{10}^+$ peak reveals also an increase of contributing cluster sizes for larger clusters.

Besides the broadening of the hillock height distribution, figure 4 also shows an increase of the mean value of the hillocks height with increasing cluster size. This is shown in figure 6(a) with the mean height linearly decreasing as a function of the projectile energy in keV/atom which decreases with the number of atoms per cluster. The stopping power, conversely, increases with cluster size and thus the inset shows an increase of mean height versus stopping power. For the stopping power S$_n$ in the inset, the nuclear stopping was calculated for Au$_1^+$ at different energies.
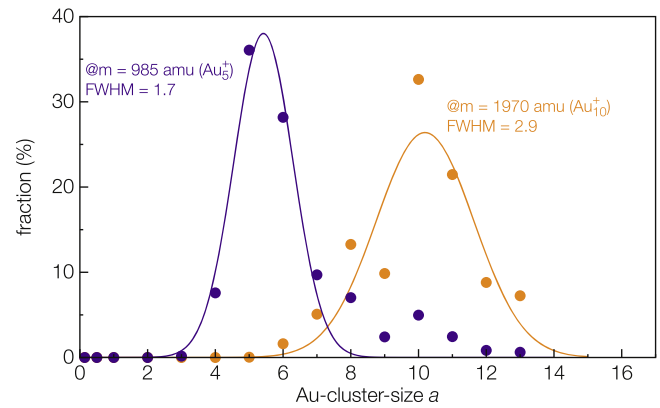

Figure 5. Cluster size spectrum for nominal sizes of Au$_5^+$- and Au$_{10}^+$-clusters. For the Au$_5^+$ peak, it is shown that not only Au$_5^+$ contribute to the ion current, but also Au$_4^+$ (~8%), Au$_6^+$ (~28%), and Au$_7^+$ (~10%). For the Au$_{10}^+$ peak even more different cluster-sizes contribute to this distribution. The data is extracted from the fit in figure 1.
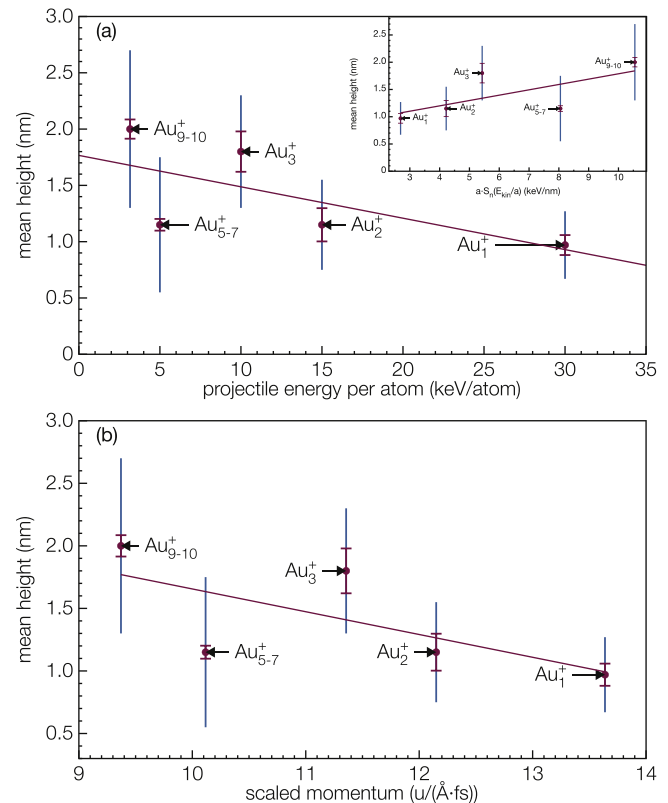

Figure 6. (a) Mean height of hillocks as a function of the projectile energy. Inserted graph shows the mean height as a function of the sum of the stopping powers for each cluster. The sum was calculated by multiplying the stopping power at E_{kin}/a with a, where a is the cluster-size. (b) shows the hillock height vs. scaled momentum, calculated as suggested in [37]. The blue lines represent the width of the distribution (FWHM), whereas the red error bars represent the error of the mean value (in this case $\frac{3 \cdot \sigma}{\sqrt{N}}$; N: number of hillocks; σ: standard deviation).

Considering that the kinetic energy is distributed equally to the atoms of the cluster, each atom has a certain stopping power dependent on its initial energy $E_{kin}(Au_1)/a$ where a is the corresponding cluster-size. Thus by multiplying stopping

power of Au_1^+ for the respective kinetic energies with a, the stopping power of each cluster is calculated (see also supplementary figure 3).

Hence, in figure 6, we find that with decreasing energy per atom, the energy deposition takes place closer to the surface, which increases the height of the nano-hillocks. This is comparable to estimations using TRIM [38] for monomere Au atoms, where the ion range into the target is also connected to the projectile energy (16.4 nm for 30 keV/179 amu compared to 6.6 nm for 5 keV/179 amu). Applying the scaling relation proposed by Seminara *et al* [37], one can see in figure 6(b) that a there is a correlation of hillock height and scaled momentum. To calculate the scaled momentum, the clusters are approximated with spheres. The volume of the cluster is filled with N-spheres, where the atomic radius of each individual sphere is the 'Wigner Seitz radius'. This radius is defined by:

$$r_{ws} = \sqrt[3]{\frac{3M_{at}}{4\pi\rho_0}}, \qquad (1)$$

where M_{at} is the mass of the atom and ρ_0 the density of the bulk. By dividing the momentum of the cluster ion by $N^{\frac{2}{3}} r_{ws}^2 \pi$ the scaled momentum, which is scaled by the cluster projected surface, can be obtained. In contrast to (a) where the height is discussed solely in regard to the energy per atom, the scaled momentum combines mass and energy in one parameter. This proves to be a promising parameter to relate to the hillock height on CaF_2 by Au-cluster irradiation in dependence of the acceleration potential, regardless of the cluster size.

For a better understanding of the results presented above, the processes taking place and creating the hillocks are put into context with existing results [9, 17, 18, 21]. We first discuss the mechanism of nano-hillock-formation induced by slow HCIs (5 keV kinetic energy, i.e. $150 \times$ q eV Xe^{33+} [17], where q is the charge state of the HCI). The energy deposition of an impinging ion in a target is composed by the sum of the nuclear stopping power S_n, the electronic stopping power S_e and the deposition of potential energy. While the nuclear stopping can be seen as the direct transfer of kinetic energy into the lattice, e.g. direct knock-on impact on target atoms leading to an excitation of phonons and quasi-free recoils along the projectile trajectory, the electronic stopping and potential energy release can be seen as a measure of excitation of the electronic subsystem of the target. Slow HCIs possess a potential energy, composed by the sum of the ionization energies of the 'missing' electrons. Since the contribution of electronic stopping to nano-hillock formation is found to be negligible for slow HCIs (only about 5% [17]) and the total stopping power only amounts to about 1.3 keV nm^{-1}, the potential energy stored in the HCI is here responsible for the creation of nano-hillock on CaF_2 [17]. The creation process takes place as follows: the HCI approaches the surface and an electron transfer from the target into highly excited states of the projectile is initiated. This leads to a strong electronic excitation in the impact region, where subsequently lattice heating takes place via electron-phonon coupling and the material in a nano-sized area around the impact melts, often referred to as nano-melting. The nano-hillock creation is explained within the thermal spike model
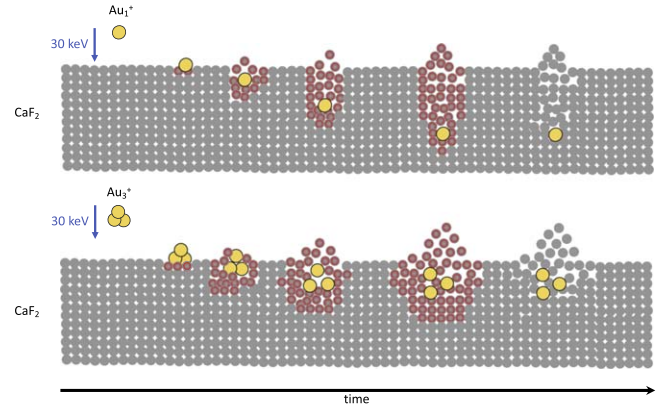

Figure 7. Schematic of direct knock-on processes. Irradiation with Au_1^+ and Au_3^+ is shown to draw a better comparison to the change of surface sensitivity with change of cluster size. Here, the energy deposition is shown as change of colour of the CaF_2 atoms. The larger the impinging particle, the more surface sensitive the energy deposition gets and hence the higher the nano-hillocks are.

[39, 40], where the molten volume thermally expands and rapidly quenches, forming small nano-hillocks.

For irradiation with Au-clusters, we propose that the creation of the nano-hillocks is induced (due to the negligible potential energy of Au_a^+) by direct knock-on processes, which is schematically shown in figure 7. When the projectile hits the target, the cluster cracks up and a dens overlap of individual collisional cascades of several heavy Au atoms proceeds (which is shown in figure 7 as a change of colour). Subsequently, phonons are excited and recoils set in motion along the trajectory of the particles, where the impinging particle collides elastically with the targets atoms. Similar to the process found for slow HCIs, a thermal expansion and rapid quenching takes place, leading to a change of material structure in a nano-sized area. This process takes place close to the surface (few nm) where visible and non-erasable nano-hillocks are formed. As it is shown in figures 6(a) and (b), cluster ions with a higher cluster size form higher nano-hillocks compared to smaller ones. This is due to the higher energy per atom and a higher scaled momentum for smaller clusters, since all irradiations were performed with the same acceleration voltage, implying that the energy deposition occurs closer to the target surface the heavier the cluster is. The total deposited energy is always the same and amounts to 30 keV. Therefore, we see in figures 6(a) and (b), that Au_{9-10}^+-clusters create higher nano-hillocks than Au_{5-7}^+, Au_3^+, Au_2^+ and Au_1^+, because the total stopping power is the highest for Au_{10}^+. In other words, with increasing cluster size and hence increasing nuclear stopping power and decreasing scaled momentum, the height of created hillocks was found to increase as well, which can be seen in the inset in figures 6(a) and (b). The height ranges from 1 nm (Au_1^+) up to 2 nm (Au_{10}^+). These values are in good agreement to the ones found after irradiation with slow HCIs (0.5–1.5 nm [18, 19]), where the potential energy and hence the charge state of the HCIs was used to tune the fabrication of nano-structures. This also agrees well with the results found in [1, 2], and references
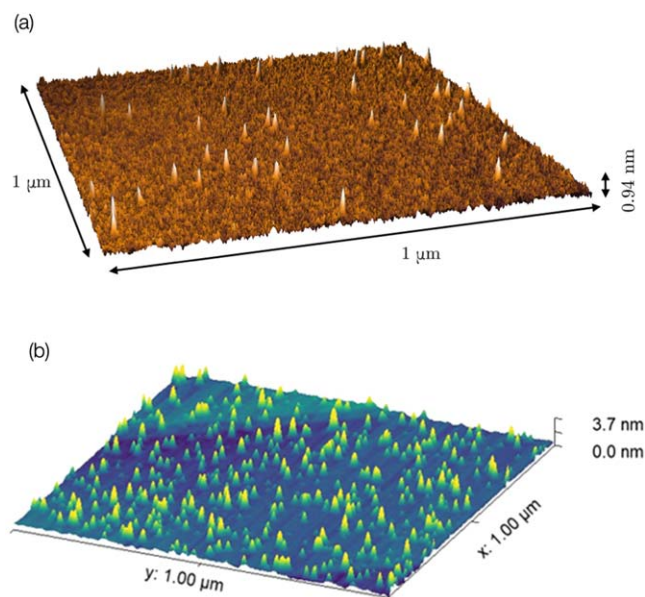
Figure 8. Comparison of 3D-plots of AFM images after irradiation with (a) highly charged ions (non-published image from [41]) and (b) after irradiation with Au_{5-7}-clusters.

therein, where an increasing penetration depth is observed with increasing scaled momentum, highlighting the observed connection between surface sensitivity and energy deposition. Figure 8 shows the comparison of a $CaF_2(111)$ surfaces irradiated Xe^{33+} (a) and with Au_{5-7}^+-clusters (b). It should be mentioned here, that also 30 keV Au monomeres create hillocks efficiently. Comparing the energy needed to melt CaF_2 (0.55 eV/atom), the energy per recoil already exceeds this threshold for Au_1^+ with roughly 38.7 eV/atom (mean value of energy per recoil at the mean projectile range, simulated with TRIM [38]). In contrast to hillocks induced by HCIs, the interaction volume of the impinging cluster with the surface material is more localized, since no electron-phonon coupling (and hence energy-dissipation throughout a larger volume) takes place with cluster irradiation. We did not observe crater formation induced by cluster irradiation, which was observed by Popok *et al* [2] for 18 keV Ar_{12}^+ cluster irradiation on Si. Contrary to the thermal conductivity of Si (148 $W\,m^{-1}\,K^{-1}$), the one of CaF_2 (9.71 $W\,m^{-1}\,K^{-1}$) is significantly smaller, hence leading to a more local melting and therefore to a hillock formation rather than a crater formation. We did not observe a threshold in cluster size for hillock creation, because the energetic heavy monomere projectiles induce an energetic cascade in CaF_2. The picture may change at lower total energy or energy per atom.

4. Conclusion

Our results show the possibility to create nano-hillocks on $CaF_2(111)$ surfaces with Au-cluster-irradiation. The resulting structures are very similar to the ones observed previously with slow HCIs. Most importantly, we have shown for the first time that we can fine-tune the height of the hillocks by changing the cluster size or energy of the impinging projectile, which is essential for further studies regarding nanofabrication of structures on different surfaces.

Data availability statement

The data generated and/or analysed during the current study are not publicly available for legal/ethical reasons but are available from the corresponding author on reasonable request.

ORCID iDs

Gabriel L Szabo https://orcid.org/0000-0002-9203-4253
Lothar Bischoff https://orcid.org/0000-0003-3968-7498
Friedrich Aumayr https://orcid.org/0000-0002-9788-0934
Nico Klingner https://orcid.org/0000-0001-9539-5874
Richard A Wilhelm https://orcid.org/0000-0001-9451-5440

References

[1] Popok V N 2011 *Mater. Sci. Eng.* R **72** 137
[2] Popok V N, Barke I, Campbell E E B and Meiwes-Broer K 2011 *Surf. Sci. Rep.* **66** 347
[3] Aumayr F, Facsko S, El-Said A, Trautmann C and Schleberger M 2011 *J. Phys.: Condens. Matter.* **23** 393001
[4] Wilhelm R A, El-Said A, Krok F, Heller R, Gruber E, Aumayr F and Facsko S 2015 *Prog. Surf. Sci.* **90** 377
[5] Meiwes-Broer K (ed) 2000 *Metal Clusters at Surfaces* (Berlin: Springer)
[6] Valbusa U, Boragno C and de Mongeot F B 2002 *J. Phys.: Condens. Matter.* **14** 8153
[7] Ziegler J F, Biersack J P and Littmark U (ed) 2008 *The Stopping and Range of Ions in Matter* (New York: Pergamon)
[8] Popok V N, Prasalovich S V and Campbell E E B 2004 *Vacuum* **76** 265
[9] Popok V N, Prasalovich S V and Campbell E E B 2003 *Nucl. Instr. Methods* B **207** 145
[10] Song J H, Choi D K and Choi W K 2002 *Nucl. Instr. Methods* B **196** 275
[11] Song J H and Choi W K 2002 *Nucl. Instr. Methods* B **190** 792
[12] Pratontep S, Preece P, Xirouchaki C, Palmer R E, Sanz-Navarro C F, Kenny S D and Smith R 2003 *Phys. Rev. Lett.* **90** 055503
[13] Prasalovich S, Popok V and Campbell E E B 2005 *Eur. Phys. J.* D **36** 79
[14] Aumayr F, Kurz H, Schneider D, Briere M A, McDonald J W, Cunningham C and Winter H 1993 *Phys. Rev. Lett.* **71** 1943

[15] Aumayr F, El-Said A and Meissl W 2008 *Nucl. Instr. Methods* B **266** 2729

[16] Pomeroy J M, Perrella A C, Grube H and Gillaspy J D 2007 *Phys. Rev.* B **75** 241409

[17] El-Said A *et al* 2008 *Phys. Rev. Lett.* **100** 237601

[18] El-Said A, Meissl W, Simon M C, Crespo-López-Urrutia J R, Gebeshuber I C, Lang M, Winter H, Ullrich J and Aumayr F 2007 *Nucl. Instr. Methods* B **256** 346

[19] El-Said A, Wilhelm R A, Heller R, Sorokin M, Facsko S and Aumayr F 2016 *Phys. Rev. Lett.* **117** 126101

[20] Facsko S, Heller R, El-Said A, Meissl W and Aumayr F 2009 *J. Phys.: Condens. Matter.* **21** 224012

[21] El-Said A, Heller R, Wilhelm R A, Facsko S and Aumayr F 2014 *Appl. Surf. Sci.* **310** 169

[22] El-Said A, Wilhelm R A, Heller R, Akhmadaliev S and Facsko S 2013 *Nucl. Instr. Methods* B **317** 170

[23] El-Said A, Wilhelm R A, Heller R and Facsko S 2019 *Nucl. Instr. Methods* B **317** 137

[24] Gruber E *et al* 2016 *J. Phys.: Condens. Matter.* **28** 405001

[25] Khalfaoui N, Görlich M, Müller C, Schleberger M and Lebius H 2006 *Nucl. Instr. Methods* B **245** 246

[26] Jensen J, Dunlop A and Della-Negra S 1998 *Nucl. Instr. Methods* B **141** 753

[27] Müller C, Cranney M, El-Said A, Ishikawa N, Iwase A, Lang M and Neumann R 2002 *Nucl. Instr. Methods* B **191** 246

[28] Alencar I *et al* 2021 *Appl. Surf. Sci.* **537** 147821

[29] Trautmann C, Toulemonde M, Schwartz K, Constantini J M and Müller A 2000 *Nucl. Instr. Methods* B **164** 365

[30] Akcöltekin E, Akcölketin S, Osmani O, Duvenbeck A, Lebius H and Schleberger M 2008 *New J. Phys.* **10** 053007

[31] Toulemonde M, Dufour C, Meftah A and Paumier E 2000 *Nucl. Instr. Methods* B **166** 903

[32] Lang M, Lian J, Zhang J, Zhang F, Weber W J, Trautmann C and Ewing R C 2009 *Phys. Rev.* B **79** 224105

[33] Wen C, Banshchikov A G, Illarionov Y Y, Frammelsberger W, Knobloch T, Hui F, Sokolov N S, Grasser T and Lanza M 2020 *Adv. Mater.* **32** 2002525

[34] Wei Y *et al* 2018 *Adv. Opt. Mater.* **6** 1701343

[35] Bischoff L, Mazarov P, Bruchhaus L and Gierak J 2016 *Appl. Phys. Rev.* **3** 021101

[36] Wojdyr M 2010 *J. Appl. Cryst.* **6** 1126

[37] Seminara L, Convers P, Monot R and Harbich W 2004 *Eur. Phys. J.* D **29** 49

[38] Biersack J and Haggmark L 1980 *Nucl. Instr. Methods* **174** 257

[39] Wang Z G, Dufour C, Paumier E and Toulemonde M 1994 *J. Phys.: Condens. Matter.* **6** 6733

[40] Dufour C, Khomrenkov V, Wang Y Y, Wang Z G and Aumayr F 2017 *J. Phys.: Condens. Matter.* **29** 095001

[41] El-Said A, Wilhelm R A, Heller R, Facsko S, Lemell C, Wachter G, Burgdörfer J, Ritter R and Aumayr F 2012 *Phys. Rev. Lett.* **109** 117602